Pharmaceutical Research, Vol. 22, No. 4, April 2005 (© 2005)
10.1007/s11095-005-2503-0

Research Paper

Molecular Cloning and Functional Analyses of OAT1 and OAT3 from Cynomolgus Monkey Kidney

Harunobu Tahara,[1,2] Masayuki Shono,[1] Hiroyuki Kusuhara,[1] Hajime Kinoshita,[1] Eiichi Fuse,[2] Akira Takadate,[3] Masaki Otagiri,[4] and Yuichi Sugiyama[1,5]

Received September 20, 2004; accepted January 10, 2005

Purpose. The functional characterization of monkey OAT1 (*SLC22A6*) and OAT3 (*SLC22A8*) was carried out to elucidate species differences in the OAT1- and OAT3-mediated transport between monkey and human.
Methods. The cDNAs of monkey OAT1 and OAT3 were isolated from monkey kidney, and their stable transfectants were established in HEK293 cells (mkOAT1- and mkOAT3-HEK). Transport studies were performed using cDNA transfectants, and kinetic parameters were compared among rat, monkey and human.
Results. The amino acid sequences of mkOAT1 and mkOAT3 exhibit 97% and 96% identity to their corresponding human orthologues. For OAT1, there was no obvious species difference in the K_m values and the relative transport activities of 11 substrates with regard to *p*-aminohippurate transport. For OAT3, there was no species difference in the K_m values and in the relative transport activities of nine substrates with regard to benzylpenicillin transport between monkey and human. However, the relative transport activities of indoxyl sulfate, 3-carboxy-4-methyl-5-propyl-2-furanpropionate, and estrone-3-sulfate showed a difference between primates and rat and gave a poor correlation.
Conclusion. These results suggest that monkey is a good predictor of the renal uptake of organic anions in the human.

KEY WORDS: OAT1; OAT3; organic anion transporter; species differences.

INTRODUCTION

The pharmacokinetics of drugs play an essential part in their pharmacological/toxicological effects. *In vitro* scaling methods have been developed to predict pharmacokinetics in human and to select candidate drugs with appropriate pharmacokinetic properties. The monkey has been used in pharmacological, toxicological, and pharmacokinetic studies in many pharmaceutical companies and is recognized as an animal model suitable for validation of such *in vitro* scaling methods, as it is the second nearest species to the human in the evolutionary tree. In order to understand the species difference in enzymological properties between monkey and human, intensive cloning and functional analyses of monkey cytochrome P450s in the liver have been performed (1–3). The cumulative results suggest that it is not necessarily appropriate to conclude that the metabolic activities exhibited by monkey P450s are similar to those in human, and the difference in the enzymatic activities per unit enzyme and/or expression levels needs to be taken into consideration in some cases (4,5).

The renal excretion of a drug involves glomerular filtration, active tubular secretion, and reabsorption. It has been shown that simple allometric scaling of clearance provides a good predictability for drugs the elimination of which is governed by physiologic parameters (glomerular filtration rate and blood flow), as these parameters can be described by an allometric equation (6,7). Several β-lactam antibiotics mainly eliminated by glomerular filtration and renal tubular secretion exhibit good allometric relationships between renal clearance based on their free serum concentrations and body weight (8), whereas there are exceptional compounds, such as

[1] Graduate School of Pharmaceutical Sciences, University of Tokyo, Hongo, Bunkyo-ku, Tokyo, 113-0033, Japan.
[2] Pharmaceutical Research Institute, Kyowa Hakko Kogyo Co., Ltd., Nagaizumi-cho, Sunto-gun, Shizuoka 411-8731, Japan.
[3] Daiichi College of Pharmaceutical Sciences, Minami-ku, Fukuoka 815-0037, Japan.
[4] Department of Biopharmaceutics, Graduate School of Pharmaceutical Sciences, Kumamoto University, Kumamoto 862-0973, Japan.
[5] To whom correspondence should be addressed. (e-mail: sugiyama@mol.f.u-tokyo.ac.jp)

ABBREVIATIONS: α-KG, α-ketoglutarate; ACV, acyclovir; AZT, 3′-azido-3′-deoxythymidine; CMD, cimetidine; CMPF, 3-carboxy-4-methyl-5-propyl-2-furanpropionate; 2,4-D, 2,4-dichloro-phenoxyacetate; DHEAS, dehydroepiandrosterone sulfate; $E_2$17βG, estradiol-17β-glucuronide; E1S, estrone-3-sulfate; HA, hippurate; HEK293, human embryonic kidney; hOAT, human organic anion transporter; IA, indoleacetate; IS, indoxyl sulfate; mkOAT, monkey organic anion transporter; MTX, methotrexate; NSAIDs, nonsteroidal anti-inflammatory drugs; OTA, ochratoxin A; PAH, *p*-aminohippurate; PCG, benzylpenicillin; rOat, rat organic anion transporter; TBS-T, tris-buffered saline/Tween 20.

betamipron and enprofyllin, the renal clearance of which was greater than the predicted values (9). Therefore, it is necessary to understand the molecular characteristics of renal transporters in order to predict human parameters more accurately from animal studies. The current study concentrated on the organic anion transporters involved in the renal uptake process and was aimed at examining the interspecies difference between monkey and human to confirm whether monkey is an appropriate *in vivo* model of the human for examining the renal elimination of drugs.

The renal uptake of organic anions on the basolateral membrane of the proximal tubules in the human has been characterized by three multispecific organic anion transporters (hOAT1-3/*SLC22A6*-*SLC22A8*) (10–12). Of these transporters, the mRNA expression level of hOAT3 determined by quantitative real-time polymerase chain reaction (RT-PCR) was the highest followed by hOAT1, while that of hOAT2 was quite low (13). The substrates of Oat1/OAT1 include various drugs, such as PAH, ochratoxin A, nonsteroidal anti-inflammatory drugs, β-lactam antibiotics, diuretics, methotrexate and antiviral drugs, and endogenous compounds, such as cyclic nucleotides, prostaglandins, uremic toxins, and dicarboxylates, while the substrates of Oat3/OAT3 include drugs, such as β-lactam antibiotics (benzylpenicillin), HMG-CoA reductase inhibitors (pravastatin) and H_2 receptor antagonists (cimetidine), and endogenous compounds, such as uremic toxins, and conjugated steroids (DHEAS, $E_2$17βG and E1S) (14–18). Based on kinetic analyses using rat kidney slices, it has been proposed that the renal uptake of hydrophilic organic anions with a low molecular weight is mainly accounted for by rOat1, while that of more bulky organic anions is by rOat3 (14–16). Because the known substrates of hOAT2 are also substrates of hOAT1 (12), and the mRNA expression in the kidney is low compared with the other two isoforms (13), the contribution of hOAT2 to the renal uptake of common substrates is likely to be small.

In the current study, we have cloned cDNAs of monkey organic anion transporter1 (mkOAT1) and mkOAT3 from a cynomolgus monkey kidney, and functional characterization was carried out using their stable transformants in HEK293 cells to compare their substrate specificity and transport activity with that in rats and humans.

MATERIALS AND METHODS

Materials

[^{3}H]IS (241 GBq/mmol) and [^{3}H]CMPF (241 GBq /mmol) were synthesized and purified by Perkin Elmer Life Sciences (Boston, MA, USA). [^{3}H]PAH (151 GBq/mmol), [^{3}H]E1S (2220 GBq/mmol) [^{3}H]MTX (555 GBq/mmol), and [^{3}H]$E_2$17βG (1110 GBq/mmol) were purchased from Perkin Elmer Life Sciences. [^{3}H]CMD (740 GBq/mmol), [^{3}H]IA (962 GBq/mmol), and [^{3}H]PCG (740 GBq/mmol) were purchased from Amersham Biosciences UK (Little Chalfont, Buckinghamshire, UK). [^{3}H]AZT (581 GBq/mmol) and [^{3}H]ACV (1484 GBq/mmol) were purchased from Moravec Biochemicals (Brea, CA, USA). [^{3}H]2,4-D (740 GBq/mmol) was purchased from American Radiolabeled Chemicals (St. Louis, MO, USA). Unlabeled PAH, CMD, AZT, ACV, E1S, DHEAS, and 2,4-D were purchased from Sigma-Aldrich (St. Louis, MO, USA), and unlabeled PCG was purchased from Wako Pure Chemicals (Osaka, Japan). All other chemicals were of analytical grade and commercially available.

Total RNA Extraction and RT-PCR

Male cynomolgus monkey kidney was purchased from BOZO research (Shizuoka, Japan). Total RNA was extracted using the extraction solution of ISOGEN (NIPPON GENE, Tokyo, Japan) according to the manufacturer's protocol. The RNA was used for reverse transcription with SuperScript First-Strand Synthesis System for the RT-PCR kit (Invitrogen, Carlsbad, CA,USA). One microliter of the RT reaction mixture was taken for a standard PCR (94°C for 2 min, 94°C for 15 s, 55°C for 30 s, 68°C for 2 min, for 40 cycles) using KOD plus polymerase (TOYOBO, Tokyo, Japan) with specific primers based on human OATs (OAT1 sense primer, 5′-CAGCCAAGGAGGCTGCTGTC-3′; antisense primer, 5′-AGTCAAACCTTTTAATGATG-3′, OAT3 sense primer, 5′-CACCTAGGACAGAGCAGGGACCTC-3′; antisense primer, 5′-CCTGGCTAGGATCAGTCTCT-3′). The PCR-products were recovered into the pENTR vector (Invitrogen) followed by a transfer to pcDNA3.2-DEST (Invitrogen) by *in vitro* recombination. The nucleotide sequences reported in this article have been submitted to the EMBL/GenBank with accession numbers AB182992 (mkOAT1) and AB182993 (mkOAT3).

Establishment of Monkey OAT1- and OAT3-Expressing HEK293 Cells

Monkey OAT1- and monkey OAT3-expressing HEK293 cells (mkOAT1- and mkOAT3-HEK) were established by introduction of pcDNA3.2-DEST-mkOAT1 or -mkOAT3 into HEK293 cells using TransIT-293 (Mirus Corporation, Madison, WI, USA) according to the manufacturer's protocol. The cells were maintained in selection medium containing antibiotic G418 sulfate to select gene-transfected cells. Among the G418-resistant clones, the stable transfectants expressing mkOAT1 or mkOAT3 were selected by the transport activity of [^{3}H]PAH for mkOAT1 or [^{3}H]estrone sulfate for mkOAT3.

Cell Culture

hOAT1- and hOAT3-HEK were established as described previously (14). h/mkOAT1- and h/mkOAT3-HEK were grown in DMEM (Invitrogen) supplemented with 10% fetal bovine serum, penicillin (100 U/ml), streptomycin (100 μg/ml), and G418 sulfate (400 μg/ml) at 37°C with 5% CO_2 and 95% humidity on the bottom of a dish. hOAT1-, hOAT3- and mkOAT1-, and mkOAT3-HEK were seeded in polylysine-coated 12-well plates and rOat1-, and rOat3-expressing cells were seeded in 12-well plates at a density of 1.2×10^5 cells/well.

Transport Studies

Transport studies were carried out as described previously (19). Uptake was initiated by adding medium containing compounds at the desired concentrations after cells had been washed twice and preincubated with Krebs-Henseleit buffer at 37°C for 15 min. The Krebs-Henseleit buffer consists of 118 mM NaCl, 23.8 mM $NaHCO_3$, 4.83 mM KCl, 0.96 mM KH_2PO_4, 1.20 mM $MgSO_4$, 12.5 mM HEPES, 5 mM glucose,

and 1.53 mM $CaCl_2$ adjusted to pH 7.4. The uptake was terminated at a designed time by adding ice-cold Krebs-Henseleit buffer after removal of the incubation buffer. Then, cells were washed twice with 1 ml ice-cold Krebs-Henseleit buffer followed by determination of the radioactivities associated with the cell and medium specimens. The transport study was performed in the absence of Na^+ to examine sodium-dependency of mkOAT1- and mkOAT3-mediated uptake of PAH, using Krebs-Henseleit buffer in which the NaCl and $NaHCO_3$ were isotonically replaced with LiCl and $LiHCO_3$, or choline chloride and choline bicarbonate, respectively. In order to examine a *trans*-stimulatory effect, glutarate was preloaded into the cells by preincubation for 15 min at designated concentration. After washing the cells by Krebs-Henseleit buffer, the uptake of PAH by mkOAT1 and mkOAT3 was determined.

Ligand uptake is given as the cell-to-medium concentration ratio determined as the amount of ligand associated with the cells divided by the medium concentration. Specific uptake was obtained by subtracting the uptake by vector-transfected cells (vector-HEK) from that by cDNA-transfected cells. Fitting was performed by the nonlinear least-squares method using a MULTI program (20) and the Damping Gauss Newton Method algorithm was used.

Western Blot Analysis

Anti-hOAT1 and -hOAT3 rabbit sera were purchased from Trans Genic Inc. (Kumamoto, Japan). Membrane fractions were prepared from monkey kidney according to a previously reported method (16). The membrane fractions were loaded onto a 10% SDS-polyacrylamide electrophoresis gel with a 4.4% stacking gel. The proteins were transferred to a polyvinylidene difluoride membrane (Pall, East Hills, NY, USA) which was then blocked with Tris-buffered saline containing 0.05% Tween 20 (TBS-T) and 5% skimmed milk for 24 h at 4°C. After washing with TBS-T, the membrane was incubated with anti-hOAT1or -hOAT3 serum (dilution 1:500) for 24 h at 4°C. The membrane was allowed to bind to a horseradish peroxidase-labeled anti-rabbit IgG antibody (Amersham Pharmacia Biotech, Buckinghamshire, UK) diluted 1: 5000 in TBS-T for 2 h at room temperature, followed by washing with TBS-T.

Immunofluorescence Study

Frozen sections from monkey kidney for immunofluorescence investigation were fixed in acetone (20°C). The sections were incubated with anti-hOAT1 or hOAT3 antibodies (1:500) for 24 h at 4°C, washed three times with PBS (140 mM NaCl and 10 mM phosphate, pH 7.4), and subsequently incubated with the secondary antibodies for 1 h at room temperature. The sections were then washed twice with PBS and mounted in VECTASHIELD Mounting Medium with propidium iodide (Vector Laboratories, Burlingame, CA, USA).

RESULTS

Cloning of Monkey Organic Anion Transporter 1 and 3 (mkOAT1 and mkOAT13)

Monkey orthologues of OAT1 and OAT3 cDNA were cloned by RT-PCR of the total RNA extracted from monkey kidney. The cDNA sequence of mkOAT1 consisted of a 1650 bp ORF encoding 550 amino acids which exhibited 96.9%, 89.5%, 88.4%, and 85.7% identity with the orthologues in human, rabbit, rat and mouse, respectively. There are three consensus sequences for *N*-glycosylation sites (Asn56, Asn92, and Asn356) that are predicted to be in the first hydrophilic loop and between the seventh and eighth transmembrane domains in this protein. The sequence also contains six potential protein kinase C-dependent phosphorylation sites (Ser164, Thr198, Ser254, Ser279, Ser327, and Thr513) located in the intracellular loops.

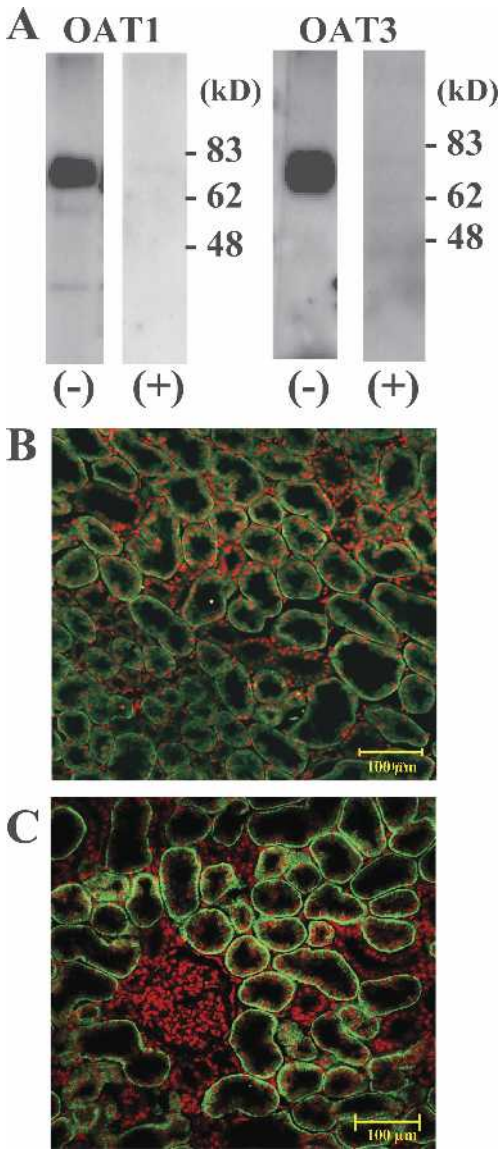

Fig. 1. Western blot analysis and immunofluorescence localization of mkOAT1 and mkOAT3. Plasma membrane fractions from cynomolgus monkey kidney was separated by SDS-PAGE (10% separating gel) with antiserum raised against hOAT1 and hOAT3 (A). mkOAT1 and mkOAT3 were detected by horseradish peroxidase-labeled anti-rabbit IgG. Immunoreactivity was abolished by pretreatment of the antibody with the antigen. Cryosections of kidney from cynomolgus monkey were incubated with hOAT1 (B) or hOAT3 (C) antiserum and stained by fluorescein isothiocyanated-labeled anti-rabbit IgG. Nucleuses were stained by propidium iodide (red). The basolateral membrane of the proximal tubule was stained by both antiserums (green fluorescence).

The cDNA sequence of mkOAT3 consisted of a 1626-bp ORF encoding 542 amino acids which exhibited 96.1%, 84.4%, 79.2%, and 77.3% identity with the orthologues in human, rabbit, rat, and mouse, respectively. There are three consensus sequences for *N*-glycosylation sites (Asn57, Asn91, and Asn356) that are predicted to be in the first hydrophilic loop and between the seventh and eighth transmembrane domains in this protein. The sequence also contains six potential protein kinase C-dependent phosphorylation sites (Ser164, Thr198, Ser254, Ser279, Ser327, and Thr513) located in intracellular loops.

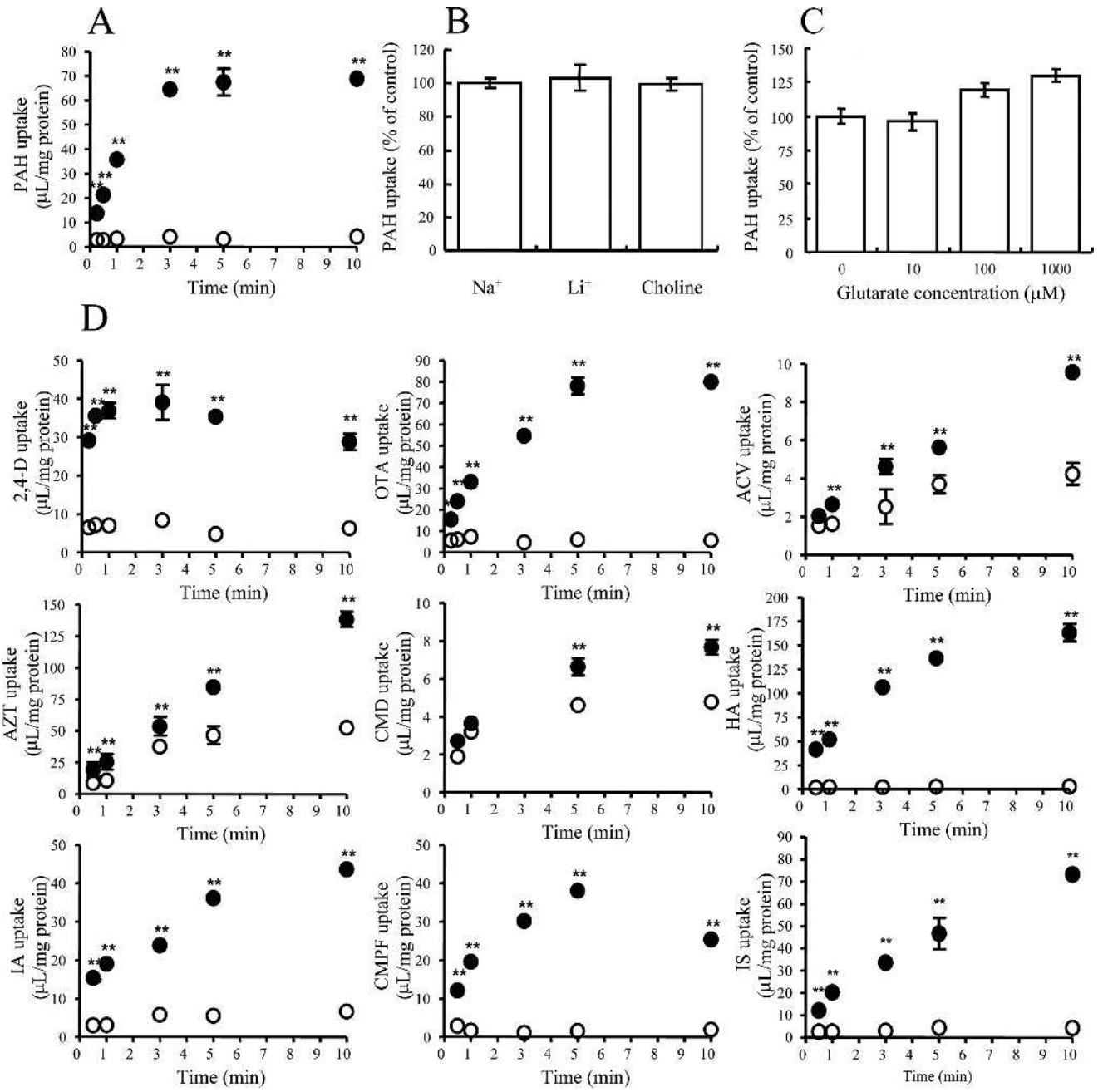

Fig. 2. Time profile, sodium dependency, and *trans*-stimulated uptake of [^{3}H]PAH and time profiles of the uptake of various compounds by mkOAT1-HEK. (A) The time-dependent uptake of [^{3}H]PAH by mkOAT1-HEK was examined at 37°C. (B) Effect of extracellular cation on [^{3}H]PAH uptake in mkOAT1-HEK. The uptake rate of [^{3}H]PAH by mkOAT1-HEK for 1 min was measured in the presence or absence of extracellular sodium. Extracellular sodium was replaced with equimolar litihium or choline. (C) *Trans*-stimulated uptake of [^{3}H]PAH by mkOAT1-HEK was preloaded with glutarate for 15 min at the indicated concentration before starting the uptake experiment. The uptake rate of [^{3}H]PAH by mkOAT1-HEK for 1 min was measured. The values were expressed as a percentage of [^{3}H]PAH uptake in mkOAT1-HEK (mean ± SE n = 3). (D) The uptake of [^{3}H] or [^{14}C]-labeled various compounds (1 μmol/L) by cDNA-transfected cells were examined at 37°C. Closed circle and open circles represent the uptake by mkOAT1-HEK and vector-HEK, respectively. Statistical differences in the uptake of mkOAT1-HEK were compared to vector-HEK by two-side unpaired Student's *t* test with $p < 0.05$ as limit of significance (*$p < 0.05$; **$p < 0.01$). Each point represents the mean ± SE (n = 3).

Expression of mkOAT1 and mkOAT3 in the Kidney

The expression of mkOAT1 and mkOAT3 in kidney plasma membrane was confirmed by Western blot analysis. As shown in Fig. 1A, mkOAT1 and mkOAT3 proteins were both detected at approximately 70 kDa in the kidney. The bands were abolished when the preabsorbed antiserum was used, suggesting that the positive bands were specific for the antigen peptide. The membrane localization of mkOAT1 and mkOAT3 in the kidney was investigated by immunofluorescence analysis. As shown in Figs. 1B and 1C, specific immunostaining for mkOAT1 (B) and mkOAT3 (C) was observed in the basolateral membrane of the proximal tubules.

Functional Characterization of mkOAT1-Mediated Transport

Transfection of mkOAT1 cDNA resulted in an increase in the uptake of PAH compared with the vector-HEK

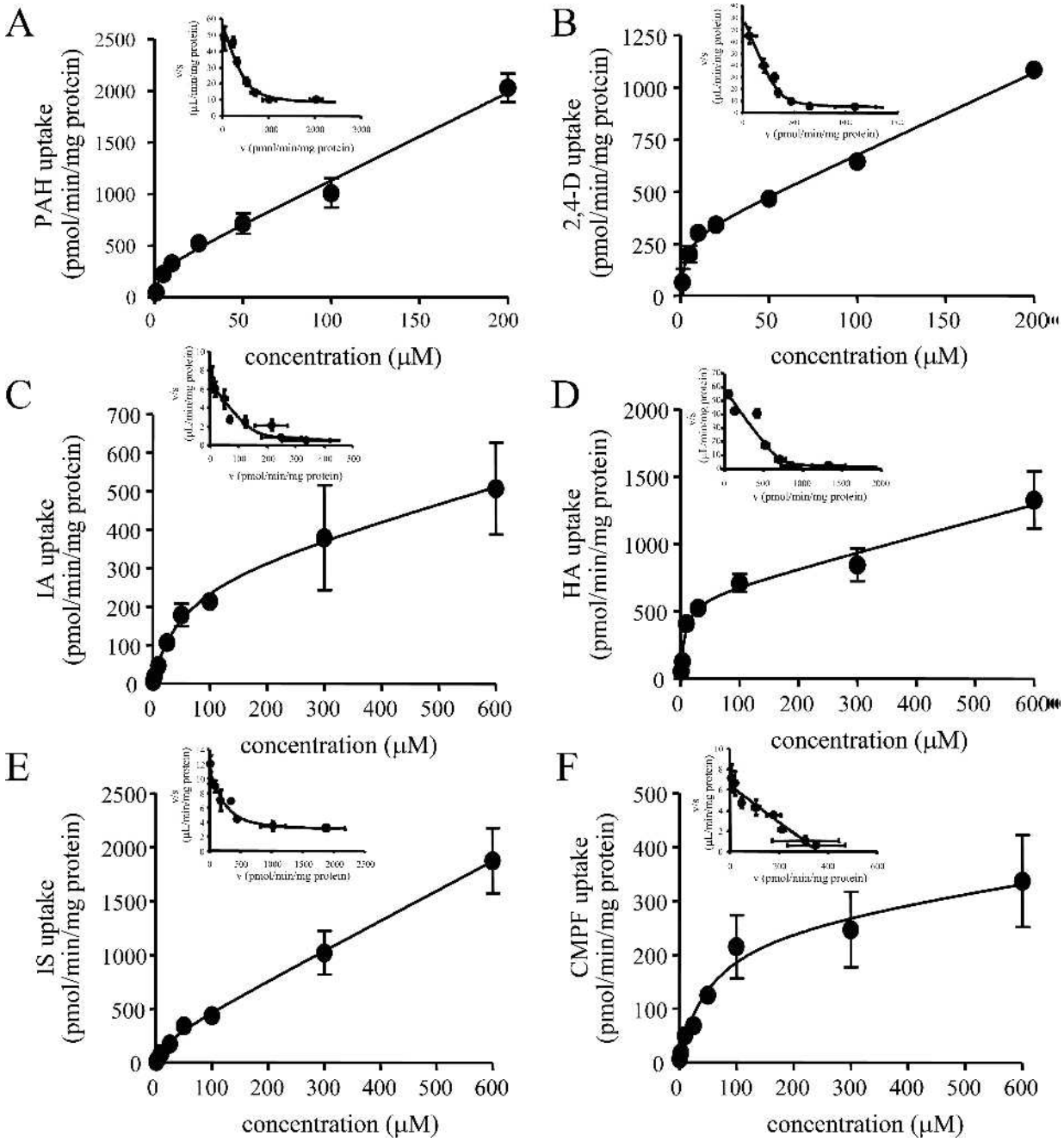

Fig. 3. Concentration dependence of the uptake of [^{3}H]PAH, [^{3}H]2,4-D, [^{3}H]IA, [^{14}C]HA, [^{3}H]IS, and [^{3}H]CMPF by mkOAT1-HEK. The concentration-dependence of mkOAT1-mediated [^{3}H]PAH (A), [^{3}H]2,4-D (B), [^{3}H]IA (C), [^{14}C]HA (D), [^{3}H]IS (E), and [^{3}H]CMPF (F) uptake were shown as Michaelis-Menten plots. The uptake of [^{3}H]PAH for 0.5 min, [^{3}H]2,4-D for 0.25 min, [^{3}H]IA for 0.5 min, [^{14}C]HA for 1 min, [^{3}H]IS for 1 min, and [^{3}H]CMPF for 1 min was determined at various concentrations (PAH; 1–200 μmol/L, 2,4,-D; 0.3–200 μmol/L, IA; 1–600 μmol/L, HA; 1–600 μmol/L IS, 0.3–600 μmol/L, and CMPF; 3–600 μmol/L; the range of concentration used). The mkOAT1-mediated transports were obtained by substracting the transport velocity in vector-HEK from those in mkOAT1-HEK. Each point represents the mean ± SE (n = 3).

Table I. Kinetic Parameters of the Uptake of Various Compounds by OAT1

	mkOAT1-HEK293			hOAT1-HEK293			rOat1-LLC-PK1		
	K_m (μmol/L)	V_{max} (pmol min^{-1} mg protein^{-1})	V_{max}/K_m (μl min^{-1} mg protein^{-1})	K_m (μmol/L)	V_{max} (pmol min^{-1} mg protein^{-1})	V_{max}/K_m (μl min^{-1} mg protein^{-1})	K_m (μmol/L)	V_{max} (pmol min^{-1} mg protein^{-1})	V_{max}/K_m (μl min^{-1} mg protein^{-1})
PAH	10.1 ± 3.2	502 ± 126	49.7 (6.57 ± 1.32)	20.4 ± 3.8	298 ± 43	14.6 (0.613 ± 0.118)	47.0 ± 5.2[c]	1330 ± 110	28.3
2,4-D	3.00 ± 1.0	272 ± 50	90.7 (5.84 ± 0.85)	5.77 ± 1.13	534 ± 32	92.6	10.2 ± 1.2[a]	1270 ± 98	125
HA	12.2 ± 2.8	702 ± 114	57.5 (0.897 ± 0.372)	23.5 ± 1.7[b]	430 ± 19	18.3	27.5 ± 4.7[b]	519 ± 69	18.9 (0.92 ± 0.15)
IA	23.6 ± 8.4	150 ± 40	6.36 (0.349 ± 0.125)	14.0 ± 8.1[b]	110 ± 50	7.86 (0.897 ± 0.224)	47.1 ± 17.3[b]	387 ± 131	8.22 (1.39 ± 0.30)
IS	32.9 ± 11.4	270 ± 85	8.21 (2.64 ± 0.34)	20.5 ± 5.3[b]	216 ± 45	10.5	17.7 ± 5.3[b]	350 ± 80	19.8 (3.42 ± 0.39)
CMPF	85.3 ± 13.3	478 ± 52	5.60	141 ± 10[b]	801 ± 45	5.67	154 ± 14[b]	1669 ± 114	10.8

K_m and V_{max} were determined by nonlinear regression analysis as described under "Materials and Methods." Data are taken from Figures 3 and 8, (a) Hasegawa *et al.* (2003), (b) Deguchi *et al.* (2004), and (c) Nagata *et al.* (2004). Each value represents the mean ± SD (n = 3). The uptake clearance of nonsaturable component was given in parentheses.

Fig. 2A). The uptake of PAH via mkOAT1 was not affected by the replacement of extracellular Na^+ with Li^+ or choline (Fig. 2B). Intracellulary accumulated glutarate by preincubating the cells in the presence of glutarate at the deisgnated concentrations significantly stimulated the uptake of PAH by mkOAT1 (Fig. 2C). In addition to PAH, the specific uptake of 2,4-D, OTA, ACV, AZT, CMD, HA, IA, CMPF, and IS by mkOAT1 was observed, while the uptake of E1S, PCG, MTX, and $E_2$17βG was comparable in vector- and mkOAT1-HEK (Fig. 2D). The concentration-dependence of the uptake of PAH, uremic toxins and 2,4-D was examined in mkOAT1-HEK (Fig. 3), and their K_m and V_{max} values, determined by nonlinear regression analysis, are summarized in Table I.

The *cis*-inhibitory effect of organic anions and cations on the mkOAT1-mediated [^{3}H]PAH uptake is shown in Fig. 4. An inhibitory effect was observed for structurally diverse organic anions and CMD, whereas an organic cation, TEA, had no effect. The inhibition potency of the inhibitors of mkOAT1-mediated transport of [^{3}H]PAH at concentration of 10 μmol/L was in the order of chlorothiazide > probenecid = bumetanide > α-ketoglutarate, furosemide > pravastatin, CMD, PCG, salicylate.

Functional Characterization of mkOAT3-Mediated Transport

Transfection of mkOAT3 cDNA resulted in an increase in the uptake of PAH compared with the vector-HEK (Fig. 5A). The uptake of PAH via mkOAT3 was not affected by the replacement of extracellular Na^+ with Li^+ or choline (Fig. 5B). Intracellulary accumulated glutarate stimulated the

Fig. 4. Inhibitory effect of organic anions and cations on the uptake of [^{3}H]PAH by mkOAT1-HEK. The uptake rate of [^{3}H]PAH by mkOAT1 for 1 min was determined in the absence or presence of inhibitors at the designed concentrations. The values were expressed as a percentage of [^{3}H]PAH uptake by mkOAT1-HEK in the presence of inhibitors vs. that in the absence of inhibitors. Each point represents the mean ± SE (n = 3).

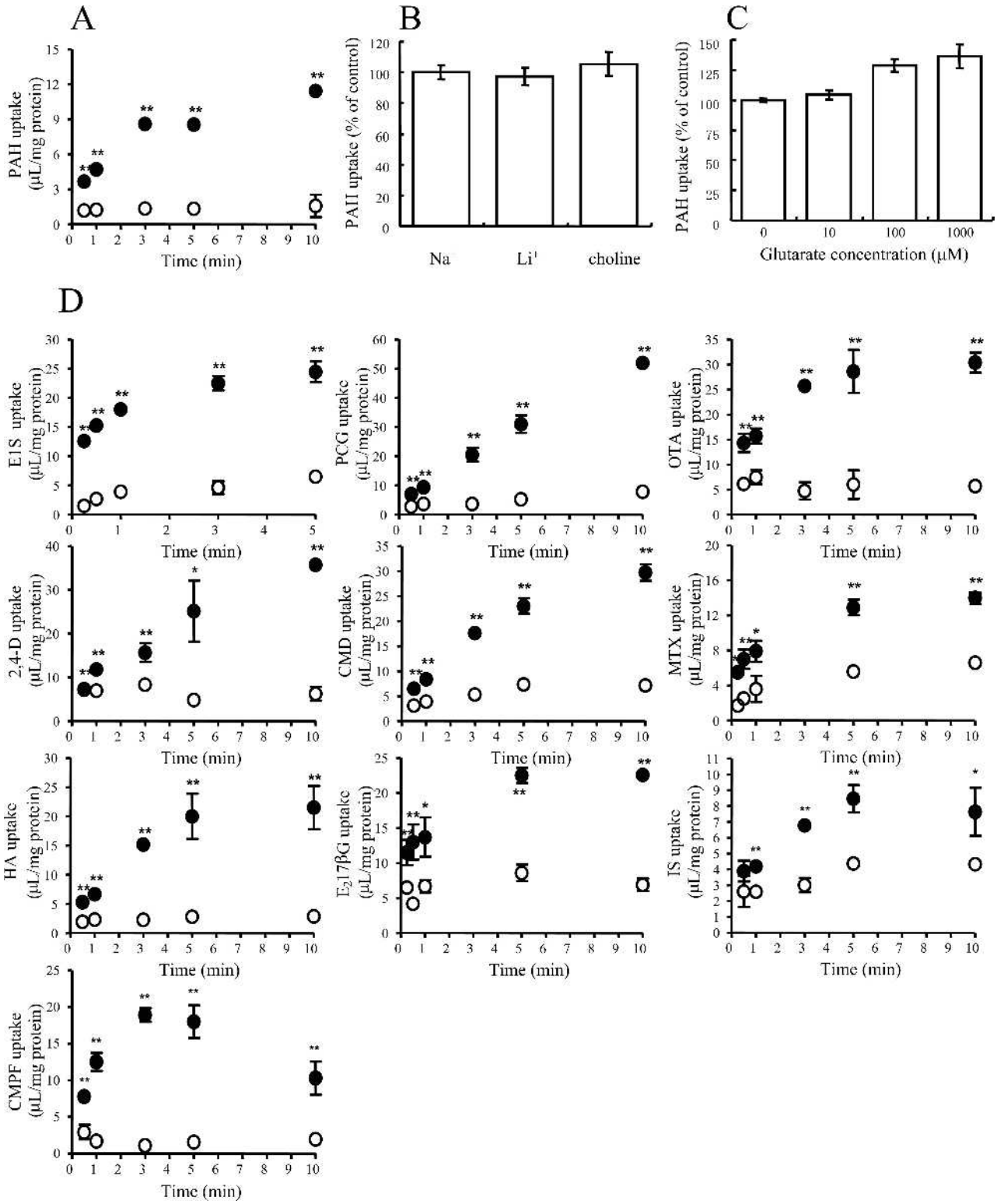

Fig. 5. Time profile, sodium dependency and trans-stimulated uptake of [^{3}H]PAH and time profiles of the uptake of various compounds by mkOAT3-HEK. (A) The time dependent uptake of [^{3}H]PAH by mkOAT3-HEK was examined at 37°C. (B) Effect of extracellular cation on [^{3}H]PAH uptake in mkOAT3- expressing HEK293 cells. The uptake rate of [^{3}H]PAH by mkOAT3-HEK for 3 min was measured in the presence or absence of extracellular sodium. Extracellular sodium was replaced with equimolar litihium or choline. (C) *Trans*-stimulated uptake of [^{3}H]PAH by mkOAT3-expressing HEK cells was preloaded with glutarate for 15 min at the indicated concentration before starting the uptake experiment. The uptake rate of [^{3}H]PAH by mkOAT3-HEK for 3 min was measured. The values were expressed as a percentage of [^{3}H]PAH uptake in mkOAT3-HEK (mean ± SE, n = 3). (D) The uptake of [^{3}H] or [^{14}C]-labeled various compounds (1 μmol/L) by mkOAT3-HEK was examined at 37°C. Closed circle and open circles represent the uptake by mkOAT3-HEK and vector-HEK, respectively. Statistical differences in the uptake of mkOAT3-HEK were compared to vector-HEK by two-side unpaired Student's *t* test with $p < 0.05$ as limit of significance (*$p < 0.05$; **$p < 0.01$). Each point represents the mean ± SE (n = 3).

uptake of PAH by mkOAT3 (Fig. 5C). In addition to PAH, the specific uptake of PCG, E1S, OTA, 2,4-D, CMD, MTX, HA, $E_2$17βG, IS, and CMPF by mkOAT3 was observed, while the uptake of IA was comparable in vector- and mkOAT3-HEK (Fig. 5D). The concentration-dependence of the uptake of PCG, E1S, CMD and CMPF by mkOAT3-HEK was examined (Fig. 6), and the K_m and V_{max} values, determined by non-linear regression analysis, are summarized in Table II.

The *cis*-inhibitory effect of organic anions and TEA on the mkOAT3-mediated PCG uptake is shown in Fig. 7. An inhibitory effect was observed for structurally diverse organic anions while TEA had no effect. The inhibition potency of the mkOAT3-mediated transport of PCG at concentration of 10 μmol/L exhibited a rank order of probenecid, furosemide = bumetanide > pravastatin > chlorothiazide = α-ketoglutarate > PAH.

Functional Characterization of hOAT1 and hOAT3

Time profile, sodium dependency and trans-stimulated uptake of [^{3}H]PAH by hOAT1- and hOAT3-HEK, and the time-profiles of the uptake of various anionic compounds, nucleoside derivatives and CMD are shown in Figs. 8 and 9, respectively. Transfection of hOAT1 or hOAT3 cDNA resulted in an increase in the uptake of PAH compared with the vector-HEK (Figs. 8A and 9A). The uptake of PAH via hOAT1- and hOAT3-HEK was sodium-independent (Figs. 8B and 9B), and *trans*-stimulatory effect by glutarate was observed in the uptake of PAH by hOAT1- and hOAT3-HEK (Figs. 8C and 9C). A significant increase was observed in the uptake of PAH, 2,4-D, OTA, AZT, and CMD by hOAT1-HEK compared with the vector-HEK, but no significant uptake of PCG and E1S and ACV was observed (Fig. 8D). The uptake of PAH and 2,4-D by hOAT1-HEK was saturable (Fig. 8D), and the K_m and V_{max} values for their uptake are summarized in Table I. Transfection of hOAT3 cDNA resulted in a significant increase in the uptake of PCG, E1S, CMD, 2,4-D, PAH, ACV, and OTA compared with the vector-HEK, but the uptake of AZT by hOAT3-HEK was comparable with that by vector-HEK (Fig. 9D). The concentration-dependence of the uptake of PCG, E1S and CMD was examined by hOAT3-HEK (Fig. 9D), and the K_m and V_{max} values for their uptake are summarized in Table II.

Correlation of OAT1- and OAT3-Mediated Transport Activities Among Rats, Monkeys, and Humans

To correct for the difference in the expression levels in the cDNA-transfectants, the relative transport activities of OAT1 substrates with regard to PAH transport were

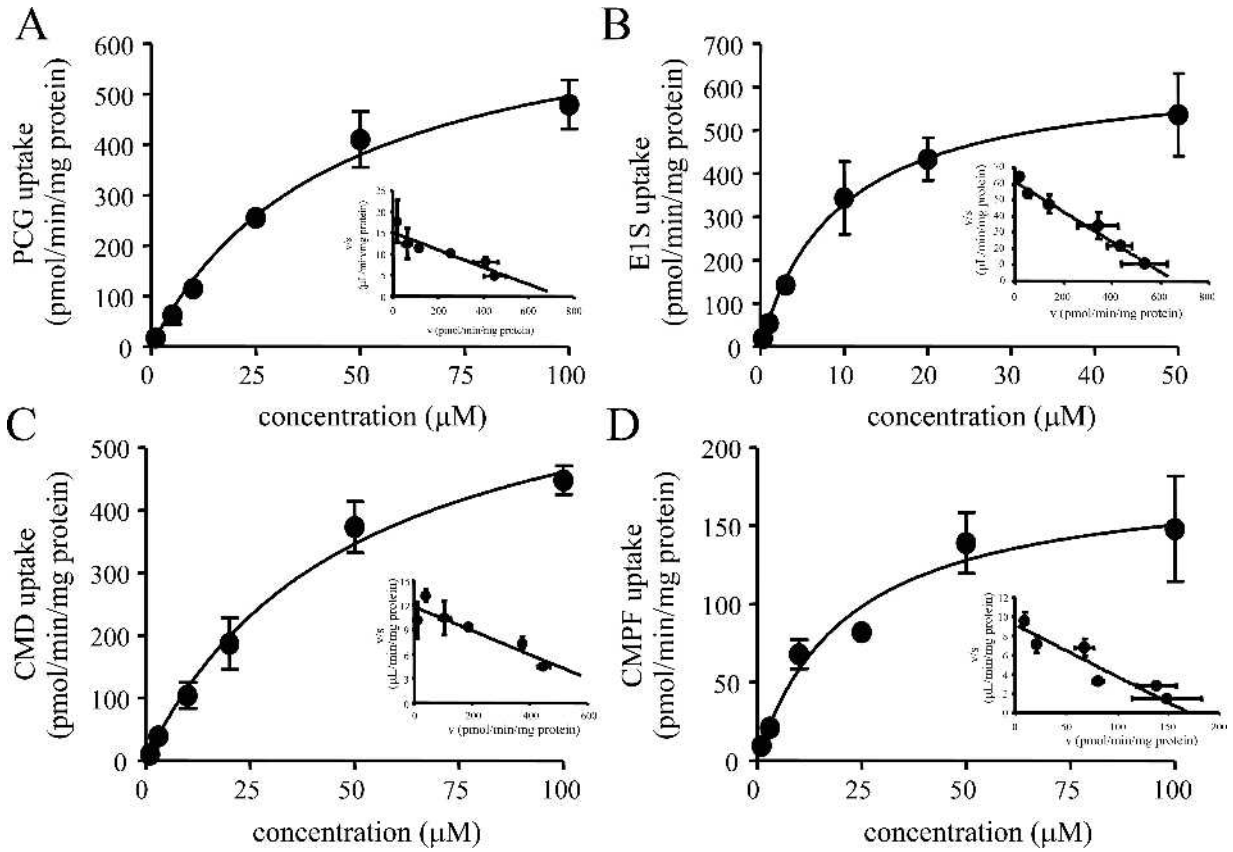

Fig. 6. Concentration dependence of the uptake of [^{3}H]PCG, [^{3}H]E1S, [^{3}H]CMD, and [^{3}H]CMPF by mkOAT3-HEK. The concentration-dependence of mkOAT1-mediated [^{3}H]PCG (A), [^{3}H]E1S (B), [^{3}H]CMD (C), and [^{3}H]CMPF (D) uptake were shown as Michaelis-Menten plots. The uptake of [^{3}H]PCG (A) for 0.5 min, [^{3}H]E1S for 0.25 min, [^{3}H]CMD for 0.5 min, and [^{3}H]CMPF for 0.5 min was determined at various concentrations (PCG; 1–100 μmol/L, E1S; 0.3–50 μmol/L, CMD; 1–100 μmol/L, and CMPF; 1–100 μmol/L; the range of concentration used). The mkOAT3-mediated transports were obtained by substracting the transport velocity in vector-HEK from those in mkOAT3-HEK. Each point represents the mean ± SE (n = 3).

Table II. Kinetic Parameters of the Uptake of Various Compounds by OAT3

	mkOAT3-HEK293			hOAT3-HEK293			rOat3-LLC-PK1		
	K_m (μmol/L)	V_{max} (pmol min^{-1} mg protein^{-1})	V_{max}/K_m (μl min^{-1} mg protein^{-1})	K_m (μmol/L)	V_{max} (pmol min^{-1} mg protein^{-1})	V_{max}/K_m (μl min^{-1} mg protein^{-1})	K_m (μmol/L)	V_{max} (pmol min^{-1} mg protein^{-1})	V_{max}/K_m (μl min^{-1} mg protein^{-1})
PCG	49.2 ± 10.6	740 ± 117	15.0	52.1 ± 14.4	194 ± 48	3.73 (0.191 ± 0.081)	85.1 ± 9.2[a]	243 ± 24	2.86
E1S	10.6 ± 0.8	663 ± 34	62.5	9.51 ± 3.07	265 ± 68	27.8 (3.60 ± 0.48)	5.32 ± 1.2[a]	39.6 ± 5.9	7.44
CMD	68.5 ± 14.7	807 ± 139	11.8	113 ± 53.8	671 ± 317	5.92 (1.12 ± 0.42)	72.4 ± 1.3[c]	150 ± 29	2.07
IS	NT	NT		263 ± 40[b]	505 ± 63	1.92	174 ± 24[b]	1047 ± 115	6.02
CMPF	18.6 ± 3.8	170 ± 22	3.84	26.5 ± 3.0[b]	198 ± 13	7.47	10.9 ± 2.0[b]	66.4 ± 9.2	6.09 (0.33 ± 0.04)

K_m and V_{max} were determined by nonlinear regression analysis as described under "Materials and Methods." Data are taken from Figures 6 and 9, (a) Hasegawa *et al.* (2003), (b) Deguchi *et al.* (2004), and (c) Nagata *et al.* (2004). Each value represents the mean ± SD (n = 3). The uptake clearance of nonsaturable component was given in parentheses. NT, not tested.

compared (Fig. 10A and 10B). A linear correlation among the species tested, hOAT1 vs mkOAT1 (A; $R^2 = 0.984$) and hOAT1 vs rOat1 (B; $R^2 = 0.946$) was observed. For OAT3, the relative transport activities of OAT3 substrates with regard to PCG transport were compared (Figs. 10C and 10D). Although a good correlation was observed between hOAT3 and mkOAT3 (C; $R^2 = 0.971$), the correlation was poor between hOAT3 and rOat3 (D; $R^2 = 0.450$).

DISCUSSION

In the current study, we reported the isolation and functional characterization of OAT1 and OAT3 from cynomolgus monkey kidney and compared the transport properties of OAT1 and OAT3 in terms of their affinity and activity in rat, monkey and human.

Cloning of mkOAT1 and mkOAT3 revealed that their amino acid sequences are quite similar to their corresponding human orthologs. Both mkOAT1 and mkOAT3 were detected in monkey kidney by Western blot at the same molecular weight as in other species (16,21,22) (Fig. 1A). They are localized on the basolateral membrane of the proximal tubules (Fig. 1B and C), which is consistent with previous reports in human (10,11).

Expression of mk/hOAT1 and mk/hOAT3 increased the uptake of PAH in HEK293 cells in a sodium-independent manner. Sodium-independence of the uptake by mk/hOAT1 and mk/hOAT3 is consistent with the previous reports in which the uptake was examined using X. laevis oocytes (10,11,23). r/hOAT1 and rOat3 are apparently dicarboxylate

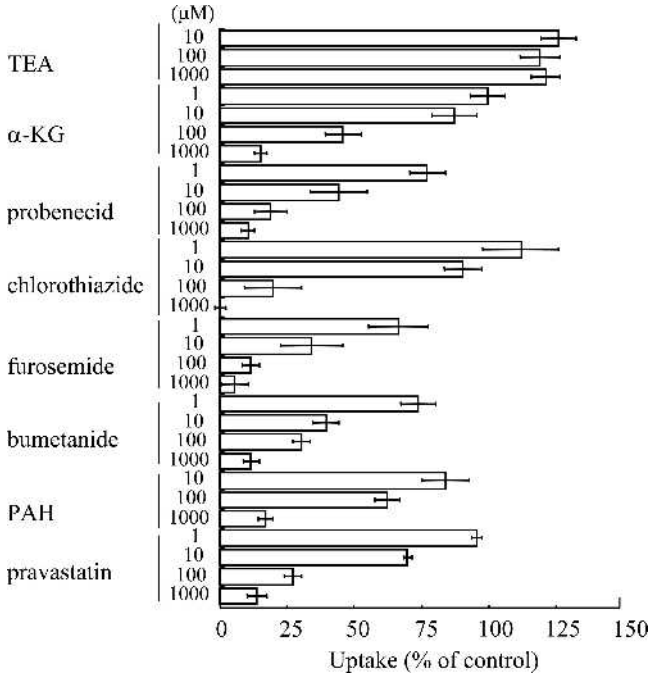

Fig. 7. Inhibitory effect of organic anions and cations on the uptake of [^{3}H]PCG by mkOAT3-HEK. The uptake rate of [^{3}H]PCG by mkOAT3 for 1 min was determined in the absence or presence of inhibitors at the designed concentrations. The values were expressed as a percentage of [^{3}H]PCG uptake by mkOAT3-HEK in the presence of inhibitors vs. that in the absence of inhibitors. Each point represents the mean ± SE (n = 3).

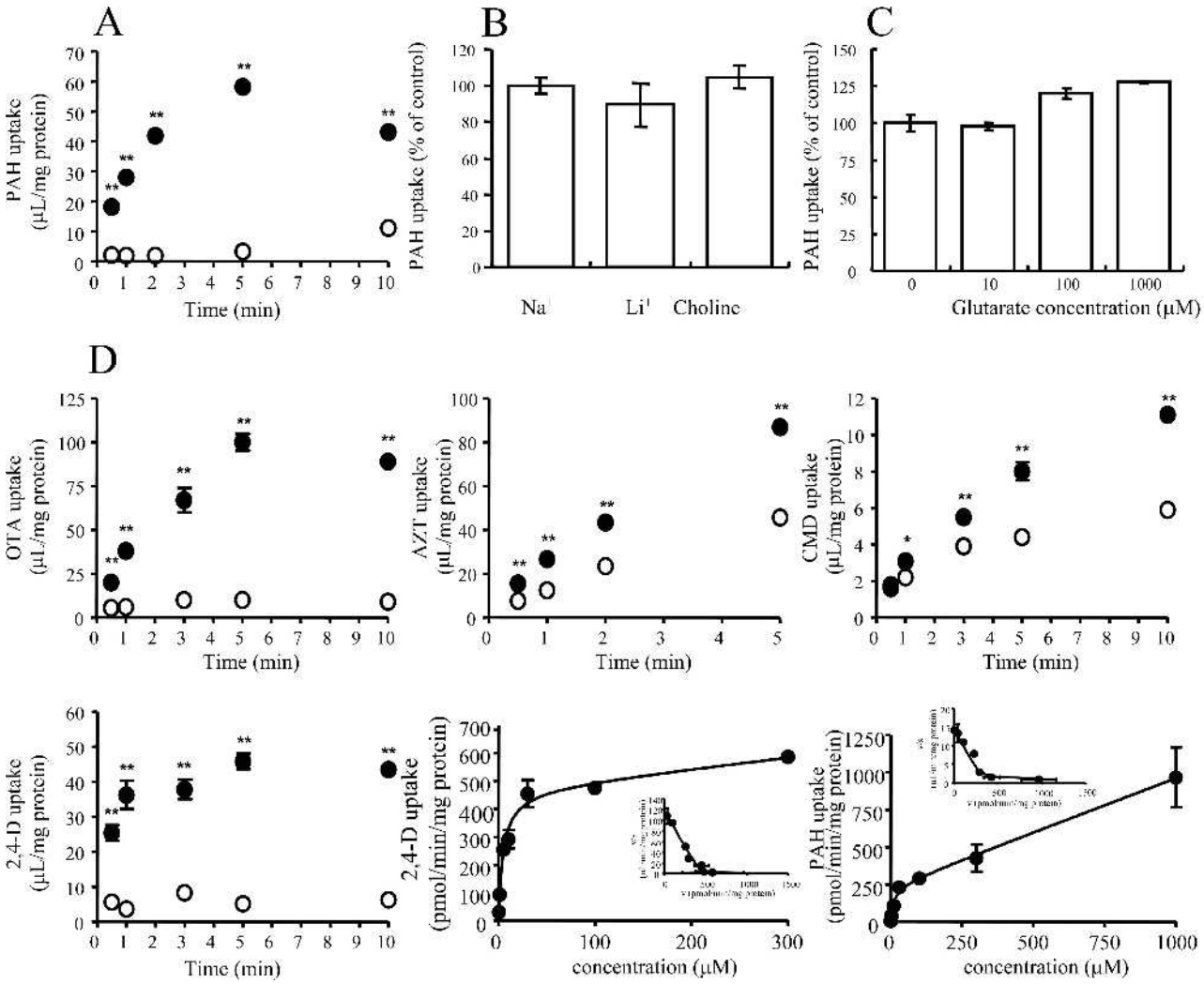

Fig. 8. Time profile, sodium dependency, and *trans*-stimulated uptake of [^{3}H]PAH and time profiles of the uptake of various compounds by hOAT1-HEK. (A) The time-dependent uptake of [^{3}H]PAH by hOAT1-HEK was examined at 37°C. (B) Effect of extracellular cation on [^{3}H]PAH uptake in hOAT1-HEK. The uptake rate of [^{3}H]PAH by hOAT1-HEK for 1 min was measured in the presence or absence of extracellular sodium. Extracellular sodium was replaced with equimolar litihium or choline. (C) *Trans*-stimulated uptake of [^{3}H]PAH by hOAT1-expressing HEK cells was preloaded with glutarate for 15 min at the indicated concentration before starting the uptake experiment. The uptake rate of [^{3}H]PAH by mkOAT1-HEK for 1 min was measured. The values were expressed as a percentage of [^{3}H]PAH uptake in hOAT1-HEK (mean ± SE n = 3). (D) The uptake of [^{3}H] or [^{14}C]-labeled various compounds (1 μmol/L) and the uptake of [^{3}H]PAH for 1 min and [^{3}H]2,4-D for 0.25 min by hOAT1-HEK were examined at various concentrations (PAH; 0.5 to 1000 μmol/L, 2,4-D; 0.3 to 300 μmol/L; the range of concentration used). Closed circle and open circles represent the uptake by hOAT1-HEK and vector-HEK, respectively. Statistical differences in the uptake of hOAT1-HEK were compared to vector-HEK by two-side unpaired Student's *t* test with $p < 0.05$ as limit of significance (*$p < 0.05$; **$p < 0.01$). Each point represents the mean ± SE (n = 3).

exchangers indirectly coupled to the sodium gradient (24–28). Intracellulary accumulated glutarate stimulated the uptake of PAH via mkOAT1- and mkOAT3-HEK to a similar degree to that observed in hOAT1- and hOAT3-HEK (Fig. 2), suggesting that both mkOAT1 and mkOAT3 are organic ion/dicarboxylate exchangers. It is speculated that the lack of any apparent sodium dependence is accounted for by the absence of a sodium-dicarboxylate cotransporter in HEK293. Indeed, Sweet *et al.* (26) demonstrated that coexpression of a sodium-dicarboxylate contransporter with rOat3 in X. *laevis* oocytes clearly induced the sodium-dependent uptake of E1S. These results suggest that mkOAT1 and mkOAT3 have transport characteristics similar to their corresponding human orthologues.

Significant uptake of typical substrates by mkOAT1 and mkOAT3 was observed (Figs. 2 and 5). The substrate specificity of mkOAT1 and mkOAT3 shows overlap although some compounds were specifically transported either by mkOAT1 or mkOAT3. 2,4-D, HA, PAH, and IS are substrates of mkOAT1, and their transport activities were markedly greater with mkOAT1 than mkOAT3, and *vice versa* for CMD. IA is a specific substrate of mkOAT1, whereas E1S, PCG, methotrexate, and $E_2$17βG were specifically transported by mkOAT3 (Figs. 2 and 5). CMPF showed similar transport activities in mkOAT1 and mkOAT3, however, the K_m value of CMPF was much smaller for mkOAT3 than for mkOAT1 (Tables I and II). An overshoot-like phenomena was observed in the uptake of 2,4-D and CMPF by mkOAT1-HEK

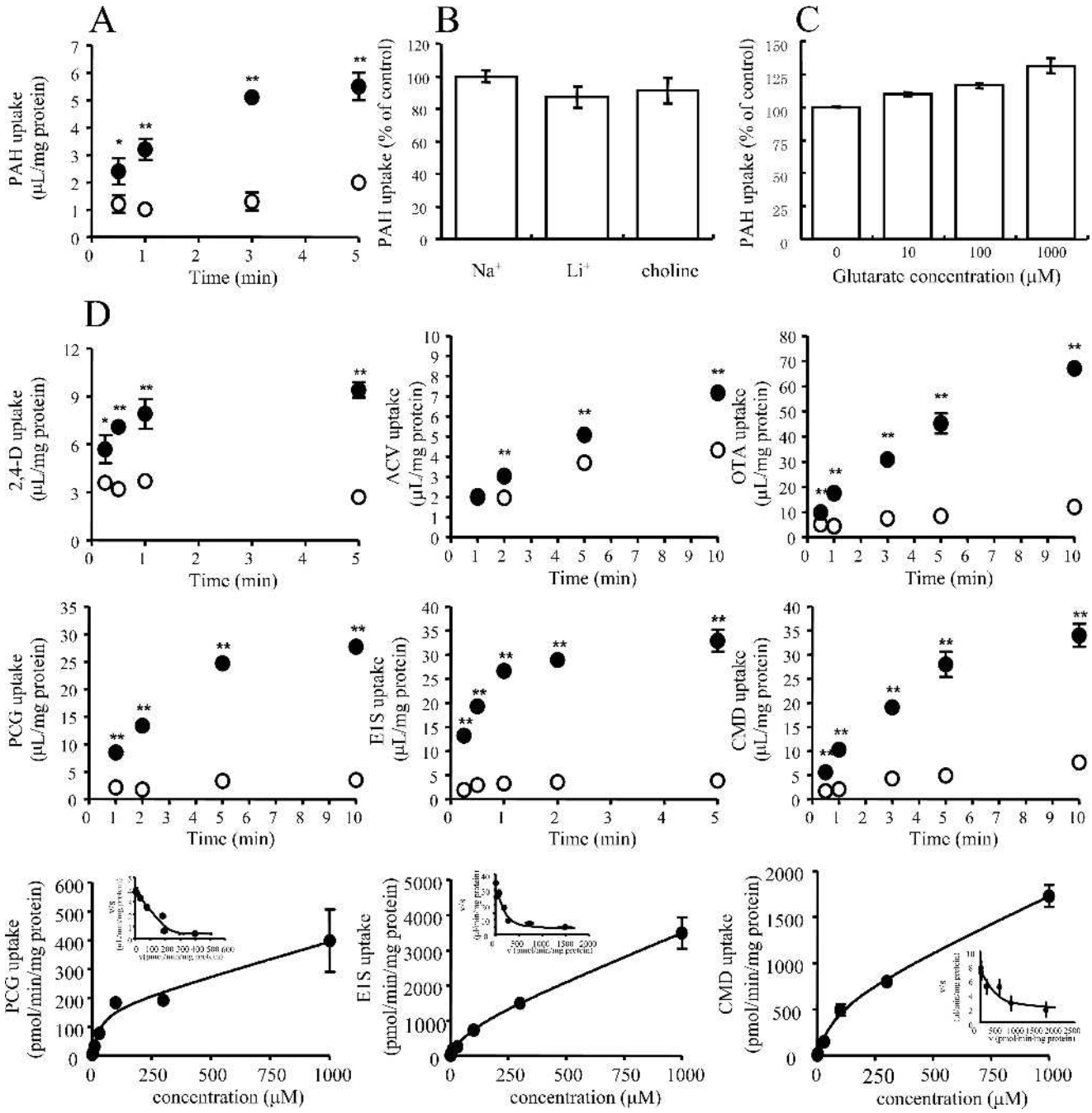

Fig. 9. Time profile, sodium dependency, and *trans*-stimulated uptake of [^{3}H]PAH and time profiles of the uptake of various compounds by hOAT3-HEK. (A) The time-dependent uptake of [^{3}H]PAH by hOAT3-HEK was examined at 37°C. (B) Effect of extracellular cation on [^{3}H]PAH uptake in hOAT3-HEK. The uptake rate of [^{3}H]PAH by hOAT3-HEK for 3 min was measured in the presence or absence of extracellular sodium. Extracellular sodium was replaced with equimolar litihium or choline. (C) *Trans*-stimulated uptake of [^{3}H]PAH by hOAT3-expressing HEK cells was preloaded with glutarate for 15 min at the indicated concentration before starting the uptake experiment. The uptake rate of [^{3}H]PAH by hOAT3-HEK for 3 min was measured. The values were expressed as a percentage of [^{3}H]PAH uptake in hOAT3-HEK (mean ± SE n = 3). (D) The uptake of [^{3}H] or [^{14}C]-labeled various compounds (1 μmol/L) and the uptake of [^{3}H]PCG for 1 min, [^{3}H]E1S for 0.25 min, and [^{3}H]CMD for 0.5 min by hOAT3-HEK were examined at various concentrations (PCG; 1 to 1000 μmol/L, E1S; 0.2 to 1000 μmol/L, and CMD 1 to 1000 μmol/L; the range of concentration used). Closed circle and open circles represent the uptake by hOAT3-HEK and vector-HEK, respectively. Statistical differences in the uptake of hOAT3-HEK were compared to vector-HEK by two-side unpaired Student's *t* test with $p < 0.05$ as limit of significance (*$p < 0.05$; **$p < 0.01$). Each point represents the mean ± SE (n = 3).

and of CMPF by mkOAT3-HEK for some unknown reason (Figs. 2 and 5). The *cis*-inhibition study showed selectivity of inhibitors for mkOAT1 and mkOAT3 (Figs. 4 and 7). α-KG and chlorothiazide are more potent inhibitors of mkOAT1 than mkOAT3, whereas furosemide and pravastatin are more potent inhibitors of mkOAT3. These inhibitors can be used to estimate the contribution of mkOAT1 and mkOAT3 to the total membrane transport process.

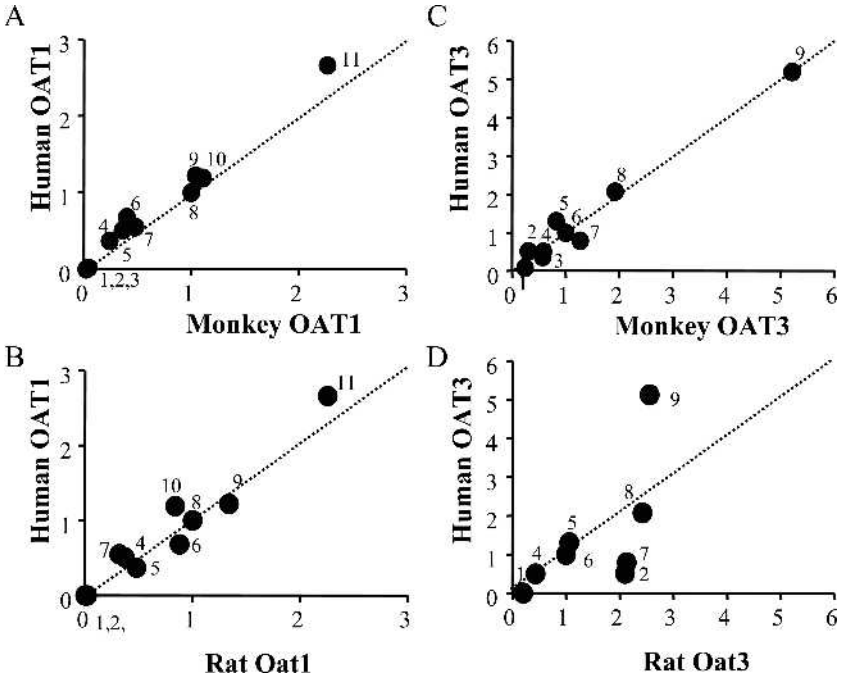

Fig. 10. Correlation of OAT1/OAT3-mediated transport activities between rats, humans, and monkeys. The correlation of OAT1-mediated relative activities between human and monkey (A) and human and rat (B). The correlation of OAT3-mediated relative activities between human and monkey (C) and human and rat (D). The relative transport activity was calculated from initial uptake velocity of tested compounds dividing by that of OAT1-mediated PAH or OAT3-mediated PCG. In every experiment, PAH and PCG were used as reference compounds to check the transport activity by OAT1- and OAT3-expressing cells. Dot line indicates correspondence 1:1. Data are taken from Figs. 2, 5, 8, and 9, Hasegawa *et al.* (2003) (15), Deguchi *et al.* (2004) (14), and Nagata *et al.* (2004) (17). (Significant correlation: A, $R^2 = 0.984$, $p < 0.01$; B, $R^2 = 0.946$, $p < 0.01$; C, $R^2 = 0.971$, $p < 0.01$. No significant correlation: D, $R^2 = 0.450$, $p > 0.05$, Pearson's correlation). OAT1 substrates: PCG(1), ACV(2), CMD(3), CMPF(4), IA(5), IS(6), AZT(7), PAH(8), OTA(9), HA(10), 2,4-D(11). OAT3 substrates: ACV(1), IS(2), 2,4-D(3), PAH(4), CMD(5), PCG(6), CMPF(7), OTA(8), E1S(9).

In order to examine the interspecies difference, the K_m values and the relative transport activities with regard to the transport activity of reference compounds (PAH for OAT1, and PCG for OAT3), were compared (Table I and Fig. 10). The K_m values for OAT1-mediated transport are comparable among the species tested (Table I), and the relative transport activities of OAT1-mediated transport with regard to the uptake of PAH exhibited a good correlation (Figs. 10A and 10B). These results suggest that there is a minimal species difference in the Oat1/OAT1-mediated transport. This is in a good agreement with a successful allometric scaling that has been reported for 2,4-D in the mouse, rat, pig, calf and human (29). 2,4-D is eliminated predominantly by the kidney (29), and its basolateral uptake has been suggested to be predominantly accounted for by rOat1 (15). Although the absolute value of the uptake is too small to affect the correlation, a species difference in CMD uptake by mk/hOAT1 and rOat1 was observed. CMD does not interact with rOat1 (30), whereas it is a poor substrate of mkOAT1 (this study) and hOAT1 (31). Therefore, difference in the amino acid sequences between primates and rat weakly affect the substrate recognition by OAT1.

As expected from high sequence homology, minimal difference was also observed for h- and mkOAT3 (Table II, Fig. 10). However, the correlation of the relative transport activities between r- and hOAT3 was poor, and E1S, CMPF and IS were out of the correlation (Fig. 10D). The relative transport activity of E1S was greater in mk/hOAT3 than in rOat3, and *vice versa* for CMPF and IS (Fig. 10D). Because relative transport activity of E1S by rOat3 with regard to benzylpenicillin uptake was similar in LLC-PK1 and HEK293 cells (data not shown), the poor correlation is presumably accounted for by the species difference, but not to the difference in the host cell line. Similar K_m values of IS and E1S between primates and rat suggests that this interspecies difference is ascribed to their V_{max} values. IS and CMPF are uremic compounds that accumulate in patients suffering from renal dysfunction, and are normally eliminated into the urine (32,33). In rats, the renal uptake of IS is equally mediated by rOat1 and rOat3, while that of CMPF is mainly accounted for by rOat3 (14). Because IS and CMPF are substrates of mkOAT1 and mkOAT3, and the E1S uptake by rat kidney slices has been suggested to be mediated by rOat3 and other unknown transporter(s) (15), such a species difference may alter the contribution of OAT1 and OAT3 in rats and primates. In addition, OAT3 has been hypothesized to account for species dependent effect of probenecid on the renal clearance of famotidine, an H_2 receptor antagonist (34,35). The renal secretion

clearance of famotidine was significantly reduced by a coadministration of probenecid in healthy volunteers (34), whereas this interaction was not observed in rats (36). Motohashi *et al.* (35) reported that famotidine is a substrate of hOAT3, but not of other basolateral transporters, hOAT1 and hOCT2, while it is a poor substrate of rOat3 (17). It is possible that the contribution of r- and hOAT3 to the renal uptake of famotidine differs between rat and human. Considering the good correlation in the relative transport activity of OAT3 between monkey and human, it is possible that the monkey is a good predictor of the drug-drug interaction.

These results suggest that the OAT1-mediated transport will be a very good predictor of renal clearance by scaling from rat to human based on an allometric equation, while the species differences in OAT3-mediated transport may be associated with a poor predictability of renal clearance in human from animal experiment, and with over- or underestimation of the contribution of the transporters. Transport studies using human cDNA transfectants are informative, however, it appears to be difficult to confirm the prediction from *in vitro* experiments because of the limited availability of human materials. Transport studies using monkey cDNA transfectants and tissue will provide a strong support for the prediction as far as the uptake process is concerned. Tubular secretion includes the efflux process at the brush border membrane as well as the uptake process at the basolateral membrane. The molecular characteristics of the monkey transporters involved in the apical excretion, which include multidrug resistance associated protein 2 (37,38), breast cancer resistant protein (BCRP) (39,40), NPT1 (41) and renal specific transporter (42), should be compared with those in human in future study to conclude that the monkey is an appropriate animal for investigating the overall tubular secretion of drugs in order to make predictions in humans.

In conclusion, we have characterized monkey multispecific OAT1 and OAT3 in terms of substrate specificity and localization in the kidney, and demonstrated that there is a minimal species difference compared with human orthologs. Taking all these findings into consideration, the monkey appears to be a better predictor of the renal uptake of exogenous organic anions in humans than in rat.

REFERENCES

1. M. Komori, O. Kikuchi, T. Sakuma, J. Funaki, M. Kitada, and T. Kamataki. Molecular cloning of monkey liver cytochrome P-450 cDNAs: similarity of the primary sequences to human cytochromes P-450. *Biochim. Biophys. Acta* **1171**:141–146 (1992).
2. T. Sakuma and T. Kamataki. A combination of monkeys and genetically engineered systems can improve the accuracy of estimations in human drug metabolism and toxicity. *Drug News Perspect.* **7**:82–86 (1994).
3. K. Ohta, M. Kitada, T. Hashizume, M. Komori, H. Ohi, and T. Kamataki. Purification of cytochrome P-450 from polychlorinated biphenyl-treated crab-eating monkeys: high homology to a form of human cytochrome P-450. *Biochim. Biophys. Acta* **996**: 142–145 (1989).
4. J. E. Sharer, L. A. Shipley, M. R. Vandenbranden, S. N. Binkley, and S. A. Wrighton. Comparisons of phase I and phase II in vitro hepatic enzyme activities of human, dog, rhesus monkey, and cynomolgus monkey. *Drug Metab. Dispos.* **23**:1231–1241 (1995).
5. J. C. Stevens, L. A. Shipley, J. R. Cashman, M. Vandenbranden, and S. A. Wrighton. Comparison of human and rhesus monkey in vitro phase I and phase II hepatic drug metabolism activities. *Drug Metab. Dispos.* **21**:753–760 (1993).
6. J. H. Lin. Species similarities and differences in pharmacokinetics. *Drug Metab. Dispos.* **23**:1008–1021 (1995).
7. R. Dedrick, K. B. Bischoff, and D. S. Zaharko. Interspecies correlation of plasma concentration history of methotrexate (NSC-740). *Cancer Chemother. Rep.* **54**:95–101 (1970).
8. H. Matsushita, H. Suzuki, Y. Sugiyama, Y. Sawada, T. Iga, M. Hanano, and Y. Kawaguchi. Prediction of the pharmacokinetics of cefodizime and cefotetan in humans from pharmacokinetic parameters in animals. *J. Pharmacobiodyn.* **13**:602–611 (1990).
9. I. Mahmood. Interspecies scaling of renally secreted drugs. *Life Sci.* **63**:2365–2371 (1998).
10. M. Hosoyamada, T. Sekine, Y. Kanai, and H. Endou. Molecular cloning and functional expression of a multispecific organic anion transporter from human kidney. *Am. J. Physiol.* **276**:F122–F128 (1999).
11. S. H. Cha, T. Sekine, J. I. Fukushima, Y. Kanai, Y. Kobayashi, T. Goya, and H. Endou. Identification and characterization of human organic anion transporter 3 expressing predominantly in the kidney. *Mol. Pharmacol.* **59**:1277–1286 (2001).
12. A. Enomoto, M. Takeda, M. Shimoda, S. Narikawa, Y. Kobayashi, T. Yamamoto, T. Sekine, S. H. Cha, T. Niwa, and H. Endou. Interaction of human organic anion transporters 2 and 4 with organic anion transport inhibitors. *J. Pharmacol. Exp. Ther.* **301**: 797–802 (2002).
13. H. Motohashi, Y. Sakurai, H. Saito, S. Masuda, Y. Urakami, M. Goto, A. Fukatsu, O. Ogawa, and K. Inui. Gene expression levels and immunolocalization of organic ion transporters in the human kidney. *J. Am. Soc. Nephrol.* **13**:866–874 (2002).
14. T. Deguchi, H. Kusuhara, A. Takadate, H. Endou, M. Otagiri, and Y. Sugiyama. Characterization of uremic toxin transport by organic anion transporters in the kidney. *Kidney Int.* **65**:162–174 (2004).
15. M. Hasegawa, H. Kusuhara, H. Endou, and Y. Sugiyama. Contribution of organic anion transporters to the renal uptake of anionic compounds and nucleoside derivatives in rat. *J. Pharmacol. Exp. Ther.* **305**:1087–1097 (2003).
16. M. Hasegawa, H. Kusuhara, D. Sugiyama, K. Ito, S. Ueda, H. Endou, and Y. Sugiyama. Functional involvement of rat organic anion transporter 3 (rOat3; Slc22a8) in the renal uptake of organic anions. *J. Pharmacol. Exp. Ther.* **300**:746–753 (2002).
17. Y. Nagata, H. Kusuhara, S. Hirono, H. Endou, and Y. Sugiyama. Carrier-mediated uptake of H2-receptor antagonists by the rat choroid plexus: involvement of rat organic anion transporter 3. *Drug Metab. Dispos.* **32**:1040–1047 (2004).
18. W. Lee and R. B. Kim. Transporters and renal drug elimination. *Annu. Rev. Pharmacol. Toxicol.* **44**:137–166 (2004).
19. D. Sugiyama, H. Kusuhara, Y. Shitara, T. Abe, P. J. Meier, T. Sekine, H. Endou, H. Suzuki, and Y. Sugiyama. Characterization of the efflux transport of 17beta-estradiol-D-17beta-glucuronide from the brain across the blood-brain barrier. *J. Pharmacol. Exp. Ther.* **298**:316–322 (2001).
20. K. Yamaoka, Y. Tanigawara, T. Nakagawa, and T. Uno. A pharmacokinetic analysis program (multi) for microcomputer. *J. Pharmacobiodyn.* **4**:879–885 (1981).
21. Y. Nagata, H. Kusuhara, H. Endou, and Y. Sugiyama. Expression and functional characterization of rat organic anion transporter 3 (rOat3) in the choroid plexus. *Mol. Pharmacol.* **61**:982–988 (2002).
22. K. Ichida, M. Hosoyamada, H. Kimura, M. Takeda, Y. Utsunomiya, T. Hosoya, and H. Endou. Urate transport via human PAH transporter hOAT1 and its gene structure. *Kidney Int.* **63**: 143–155 (2003).
23. H. Kusuhara, T. Sekine, N. Utsunomiya-Tate, M. Tsuda, R. Kojima, S. H. Cha, Y. Sugiyama, Y. Kanai, and H. Endou. Molecular cloning and characterization of a new multispecific organic anion transporter from rat brain. *J. Biol. Chem.* **274**:13675–13680 (1999).
24. A. Aslamkhan, Y. H. Han, R. Walden, D. H. Sweet, and J. B. Pritchard. Stoichiometry of organic anion/dicarboxylate exchange in membrane vesicles from rat renal cortex and hOAT1-expressing cells. *Am. J. Physiol. Renal Physiol.* **285**:F775–F783 (2003).

25. A. Bakhiya, A. Bahn, G. Burckhardt, and N. Wolff. Human organic anion transporter 3 (hOAT3) can operate as an exchanger and mediate secretory urate flux. *Cell. Physiol. Biochem.* **13**:249–256 (2003).
26. D. H. Sweet, L. M. Chan, R. Walden, X. P. Yang, D. S. Miller, and J. B. Pritchard. Organic anion transporter 3 (Slc22a8) is a dicarboxylate exchanger indirectly coupled to the Na+ gradient. *Am. J. Physiol. Renal Physiol.* **284**:F763–F769 (2003).
27. T. Sekine, N. Watanabe, M. Hosoyamada, Y. Kanai, and H. Endou. Expression cloning and characterization of a novel multispecific organic anion transporter. *J. Biol. Chem.* **272**:18526–18529 (1997).
28. D. H. Sweet, N. A. Wolff, and J. B. Pritchard. Expression cloning and characterization of ROAT1. The basolateral organic anion transporter in rat kidney. *J. Biol. Chem.* **272**:30088–30095 (1997).
29. C. Timchalk. Comparative inter-species pharmacokinetics of phenoxyacetic acid herbicides and related organic acids. evidence that the dog is not a relevant species for evaluation of human health risk. *Toxicology* **200**:1–19 (2004).
30. T. M. S. Khamdang, M. Shimoda, R. Noshiro, S. Narikawa, X. L. Huang, A. Enomoto, P. Piyachaturawat, and H. Endou. Interactions of human- and rat-organic anion transporters with pravastatin and cimetidine. *J. Pharmacol. Sci.* **94**:197–202 (2004).
31. B. C. Burckhardt, S. Brai, S. Wallis, W. Krick, N. A. Wolff, and G. Burckhardt. Transport of cimetidine by flounder and human renal organic anion transporter 1. *Am. J. Physiol. Renal Physiol.* **284**:F503–F509 (2003).
32. R. Vanholder, A. Argiles, U. Baurmeister, P. Brunet, W. Clark, G. Cohen, P. P. De Deyn, R. Deppisch, B. Descamps-Latscha, T. Henle, A. Jorres, Z. A. Massy, M. Rodriguez, B. Stegmayr, P. Stenvinkel, and M. L. Wratten. Uremic toxicity: present state of the art. *Int. J. Artif. Organs* **24**:695–725 (2001).
33. Y. Tsutsumi, T. Deguchi, M. Takano, A. Takadate, W. E. Lindup, and M. Otagiri. Renal disposition of a furan dicarboxylic acid and other uremic toxins in the rat. *J. Pharmacol. Exp. Ther.* **303**:880–887 (2002).
34. N. Inotsume, M. Nishimura, M. Nakano, S. Fujiyama, and T. Sato. The inhibitory effect of probenecid on renal excretion of famotidine in young, healthy volunteers. *J. Clin. Pharmacol.* **30**: 50–56 (1990).
35. H. Motohashi, Y. Uwai, K. Hiramoto, M. Okuda, and K. I. Inui. Different transport properties between famotidine and cimetidine by human renal organic ion transporters (SLC22A). *Eur. J. Pharmacol.* **503**:25–30 (2004).
36. J. H. Lin, L. E. Los, E. H. Ulm, and D. E. Duggan. Kinetic studies on the competition between famotidine and cimetidine in rats. Evidence of multiple renal secretory systems for organic cations. *Drug Metab. Dispos.* **16**:52–56 (1988).
37. T. P. Schaub, J. Kartenbeck, J. Konig, H. Spring, J. Dorsam, G. Staehler, S. Storkel, W. F. Thon, and D. Keppler. Expression of the MRP2 gene-encoded conjugate export pump in human kidney proximal tubules and in renal cell carcinoma. *J. Am. Soc. Nephrol.* **10**:1159–1169 (1999).
38. R. Masereeuw, S. Notenboom, P. H. Smeets, A. C. Wouterse, and F. G. Russel. Impaired renal secretion of substrates for the multidrug resistance protein 2 in mutant transport-deficient (TR-) rats. *J. Am. Soc. Nephrol.* **14**:2741–2749 (2003).
39. N. Mizuno, M. Suzuki, H. Kusuhara, H. Suzuki, K. Takeuchi, T. Niwa, J. W. Jonker, and Y. Sugiyama. Impaired renal excretion of 6-hydroxy-5,7-dimethyl-2-methylamino-4-(3-pyridylmethyl) benzothiazole (E3040) sulfate in breast cancer resistance protein (BCRP1/ABCG2) knockout mice. *Drug Metab. Dispos.* **32**:898–901 (2004).
40. J. W. Jonker, M. Buitelaar, E. Wagenaar, M. A. Van Der Valk, G. L. Scheffer, R. J. Scheper, T. Plosch, F. Kuipers, R. P. Elferink, H. Rosing, J. H. Beijnen, and A. H. Schinkel. The breast cancer resistance protein protects against a major chlorophyll-derived dietary phototoxin and protoporphyria. *Proc. Natl. Acad. Sci. USA* **99**:15649–15654 (2002).
41. A. E. Busch, A. Schuster, S. Waldegger, C. A. Wagner, G. Zempel, S. Broer, J. Biber, H. Murer, and F. Lang. Expression of a renal type I sodium/phosphate transporter (NaPi-1) induces a conductance in Xenopus oocytes permeable for organic and inorganic anions. *Proc. Natl. Acad. Sci. USA* **93**:5347–5351 (1996).
42. T. Imaoka, H. Kusuhara, S. Adachi-Akahane, M. Hasegawa, N. Morita, H. Endou, and Y. Sugiyama. The renal-specific transporter mediates facilitative transport of organic anions at the brush border membrane of mouse renal tubules. *J. Am. Soc. Nephrol.* **15**:2012–2022 (2004).